

SCIENTIFIC REPORTS

OPEN

Globally accurate potential energy surface for the ground-state HCS(X^2A') and its use in reaction dynamics

Received: 19 September 2016

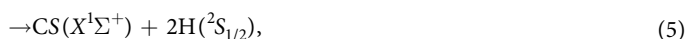
Accepted: 31 October 2016

Published: 29 November 2016

Yu-Zhi Song*, Lu-Lu Zhang*, Shou-Bao Gao & Qing-Tian Meng

A globally accurate many-body expansion potential energy surface is reported for HCS(X^2A') by fitting a wealth of accurate *ab initio* energies calculated at the multireference configuration interaction level using aug-cc-pVQZ and aug-cc-pV5Z basis sets via extrapolation to the complete basis set limit. The topographical features of the present potential energy surface are examined in detail and is in good agreement with the raw *ab initio* results, as well as other theoretical results available in literatures. By utilizing the potential energy surface of HCS(X^2A'), the dynamic studies of the $C(^3P) + SH(X^2II) \rightarrow H(^2S) + CS(X^1\Sigma^+)$ reaction has been carried out using quasi-classical trajectory method.

The HCS radical is a fundamental reaction intermediate in combustion processes¹, which plays an important role in molecular formation processes of interstellar clouds². The transient species HCS and CH_2S were identified as a reactive intermediate in hydrogen abstraction reaction of methyl mercaptane (CH_2SH) with fluorine atoms by means of photoionization mass spectroscopy³. Kaiser *et al.* demonstrated that the sulfur-containing species are important in Jupiter's atmosphere^{4,5}. They carried out experimental and theoretical studies on the reaction $C(^3P_j) + H_2S$, which has the following channels,



It should be mentioned that Cristina⁶ also studied the isomer pair HCS/HSC and related cations using the coupled cluster (CC) method in conjunction with correlation consistent basis sets ranging in size from quadruple to sextuple zeta for all the species to investigate the near-equilibrium potential energy surface (PES). In 1983, Goddard⁷ firstly predicted the equilibrium geometries of the lowest $^2A'$ and $^2A''$ electronic states of HCS using the single-double configuration interaction (SDCI) method with a double-zeta basis. Subsequently, Pope *et al.*⁸ performed a theoretical study of fragmentation and rearrangement processes of H_2CS and H_2CS^+ radicals. Moreover, the HCS/HSC and HCS^+/HSC^+ isomerizations were investigated at the CI level in conjunction with triple-zeta basis sets. Stoecklin *et al.*⁹⁻¹¹ investigated two analytic models of the lowest PES of the reaction $SH(X^2II) + C(^3P) \rightarrow H(^2S) + CS(X^1\Sigma^+)$ using the MNDO/CI method, three cols connect the HCS to HSC and ground-state

School of Physics and Electronics, Shandong Normal University, Jinan 250014, China. *These authors contributed equally to this work. Correspondence and requests for materials should be addressed to Q.-T.M. (email: qtmeng@sdu.edu.cn)

	R_e	D_e	ω_e	$\omega_e x_e$	α_e	β_e
SH($X^2\Pi$)						
MRCI(Q)/AVQZ	2.5388	-0.13827	2689.715	59.599	0.3051	9.5595
MRCI(Q)/AV5Z	2.5355	-0.13928	2695.140	59.405	0.3046	9.5844
MBE/CBS	2.5337	-0.14001	2698.763	59.254	0.3041	9.5982
Exp. ³³	2.5339	-0.13920	2695.8	59.9	0.270	9.4611
Theor. ²²	2.5354	-0.13987	2697.5	—	—	—
Theor. ²⁸	2.5325	-0.13953	2701.2	—	—	—
CH($X^2\Pi$)						
MRCI(Q)/AVQZ	2.1182	-0.13286	2842.397	69.265	0.5235	14.4307
MRCI(Q)/AV5Z	2.1171	-0.13332	2845.359	69.172	0.5229	14.4458
MBE/CBS	2.1162	-0.13374	2848.309	69.101	0.5223	14.4580
Exp. ³³	2.1170	-0.13377	2858.5	63.02	0.534	14.457
Theor. ²⁹	2.1170	-0.13326	2856.312	64.9321	0.5452	14.457
Theor. ³⁰	2.1180	-0.13285	2851.0	62.15	0.524	14.85
Theor. ³¹	2.1172	-0.13396	2860	66	0.534	14.449
CS($X^2\Sigma^+$)						
MRCI(Q)/AVQZ	2.9181	-0.27276	1270.556	6.742	0.005842	0.8102
MRCI(Q)/AV5Z	2.9114	-0.27351	1277.433	6.796	0.005880	0.8140
MBE/CBS	2.9078	-0.27432	1281.150	6.816	0.005893	0.8160
Exp. ³³	2.9016	-0.2732	1285.08	6.46	0.005922	0.8200
Theor. ³²	2.9117	-0.2699	1278.00	6.4924	0.005837	0.8144

Table 1. Spectroscopic constants of SH, CH, and CS diatoms, with the unit of R_e in a_0 , D_e in E_h , and ω_e , $\omega_e x_e$, α_e and β_e in cm^{-1} .

products. Potential energy, electric dipole and transition moment functions were calculated by Senekowitsch *et al.*¹² for the X^2A' and A^2A'' electronic states of the HCS radical at the multiconfiguration self-consistent field (MCSCF) CI level. For the X^2A' , the calculated equilibrium geometries are: $R_{\text{CH}} = 1.083 \text{ \AA}$, $R_{\text{CS}} = 1.573 \text{ \AA}$, and $\alpha_{\text{HCS}} = 131.8^\circ$, for the A^2A'' , $R_{\text{CH}} = 1.063 \text{ \AA}$, $R_{\text{CS}} = 1.557 \text{ \AA}$, and $\alpha_{\text{HCS}} = 180^\circ$, respectively. They also reported that in linear geometry the two lowest X^2A' and A^2A'' states become degenerate components of the $^2\Pi$ state and exhibit a strong Renner-Teller coupling effect. HCS, HSC, and the corresponding cationic species were also investigated by Curtiss *et al.*¹³, who carried out a theoretical study of the organo-sulfur systems CSH_n ($n = 0-4$) and CS_n ($n = 0-5$). The dissociation and ionization energies, and enthalpies of formation were calculated. Ochsenfeld *et al.*¹⁴ investigated the reaction of atomic carbon with H_2S using CC theory. In the same year, Chen *et al.*¹⁵ presented the hyperfine structures of the HCS and isovalent HCO, HSiS and HSiO radicals using the density functional theory (DFT) and multi-reference single and double excitation configuration interaction (MRSDCI) methods. In 2004, Voronin¹⁶ reported a global analytical PES corresponding to the lowest adiabatic X^2A' state of HCS using a grid of 1357 energy points calculated at the MRCI level in conjunction with the aug-cc-pVTZ basis set. By employing the PES, the main stationary points of the X^2A' surface were also evaluated. Mitrushchenkov *et al.*¹⁷ performed theoretical studies on HC_nS ($n = 1-12$) radicals in the $^2\Pi$ electronic ground state using the Hartree Fock (HF), complete active space self-consistent field (CASSCF) and MRCI methods with different basis sets. Habara *et al.*¹⁸⁻²¹ detected microwave transition of the HCS, HSC, H^{13}CS and HS^{13}C radicals in the X^2A' ground electronic state.

The major goal of the present work is to obtain an accurate global adiabatic PES for the ground state of HCS based on many-body expansion (MBE) scheme. Both aug-cc-pVQZ (AVQZ) and aug-cc-pV5Z (AV5Z) atomic basis sets have been employed. In order to improve the accuracy of PES, such obtained *ab initio* energies are then extrapolated to the complete basis-set (CBS) limit²²⁻²⁷. Based on the adiabatic PES, the reaction dynamics of $\text{C} + \text{SH}$ reaction were investigated using the quasi-classical trajectory (QCT) method.

Results

Features of HCS(X^2A') potential energy surface. Table 1 shows the characteristics of the $\text{CS}(X^1\Sigma^+)$, $\text{CH}(X^2\Pi)$ and $\text{SH}(X^2\Pi)$, including equilibrium geometries, dissociation energies, vibrational frequencies, and spectroscopic constants. Other theoretical²²⁻³² and experimental³³ values are also gathered in this table for comparison. It can be found that the present values are in good agreement with results from other literatures. The obtained in the present work equilibrium internuclear distances, vibrational constants, and dissociation energies reproduce well the available experimental and theoretical results. Shown in Fig. 1 are the $\text{CS}(X^1\Sigma^+)$, $\text{CH}(X^2\Pi)$ and $\text{SH}(X^2\Pi)$ potential energy curves (PECs). It can be seen from this figure that the modeled PECs accurately mimic the *ab initio* energies, with the maximum error being smaller than 10 cm^{-1} , which shows smooth and accurate behavior both in short and long regions. In order to evaluate the fitting quality of the present PECs, we calculate the root-mean square derivation (rmsd) using the following equation:

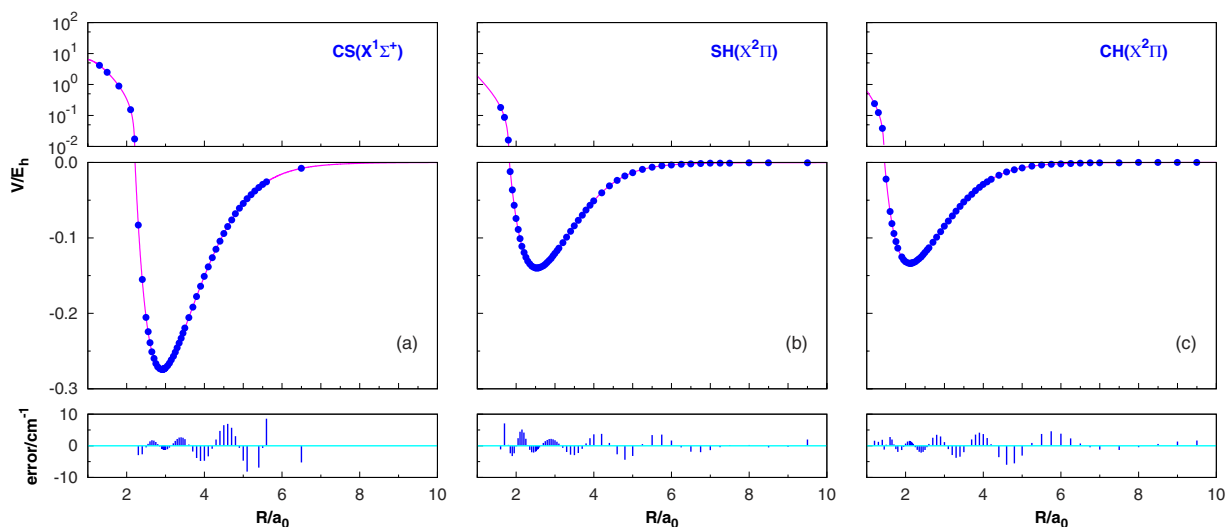


Figure 1. Potential energy curves of $\text{CS}(X^1\Sigma^+)$, $\text{SH}(X^2\Pi)$ and $\text{CH}(X^2\Pi)$, and the differences between the fit and *ab initio* points.

$$\Delta E_{\text{rmsd}} = \sqrt{\frac{1}{N} \sum_{i=1}^N [V_{\text{fit}}(i) - V_{\text{ab}}(i)]^2}, \quad (6)$$

where $V_{\text{fit}}(i)$ and $V_{\text{ab}}(i)$ are the i -th energies from fitting and from the *ab initio* calculation, respectively; N is the number of points employed in the fitting procedure. The values of ΔE_{rmsd} are 3.89, 2.03, 4.45 cm^{-1} for SH, CH, CS, respectively, which show that the fitted PECs are of a high quality.

Figure 2 illustrates the major topographical features of the $\text{HCS}(X^2A')$ PES. The salient features of these plots are the most relevant stationary points for the title system. Clearly, the variation of the contours is quite smooth in the whole configuration space. Most notable in Fig. 2(a) is the global minimum (GM) with the bending angle being fixed at its equilibrium ($\angle\alpha = 132^\circ$), which locates at $R_1 = 4.596 a_0$, $R_2 = 2.953 a_0$ and $R_3 = 2.062 a_0$ (R_1 is the SH interatomic separation, R_2 the CS interatomic separation, while R_3 the CH interatomic separation), and the well depth is $-0.3614 E_h$ relative to the $\text{H}(^2S) + \text{S}(^3P) + \text{C}(^3P)$ asymptote. In this panel, two valleys are distinguishable: the deeper one at the bottom corresponds to the $\text{H}(^2S) + \text{CS}(X^1\Sigma^+)$ asymptote, and the valley on the left corresponds to the $\text{C}(^3P) + \text{SH}(X^2\Pi)$ asymptote. Observing the Fig. 2(a), one can find that the $\text{H}(^2S) + \text{CS}(X^1\Sigma^+)$ asymptote is below the $\text{C}(^3P) + \text{SH}(X^2\Pi)$ asymptote, and it is above the global minimum. A closer observation reveals in this figure that there exists no barrier toward the dissociation of $\text{HCS}(X^2A')$ at this configuration into $\text{S}(^3P) + \text{CH}(X^2\Pi)$, and there is a transition state (TS1) connecting the global minimum with the $\text{H}(^2S) + \text{CS}(X^1\Sigma^+)$ asymptote. The different collinear configurations are shown in Fig. 2(b–d). In previous works^{5,8,16,20}, one local minimum which denoted as LM1 is reported on the PES of $\text{HCS}(X^2A')$. However, four local minima (LM1–LM4) are found on the present PES, with two of them being in linear structures. For convenience of discussion, the properties of all stationary points are collected in Table 2, including the internuclear distances, energies and vibrational frequencies. The global minimum for the HCS ground state from our CBS PES is predicted to be located at $R_1 = 4.596 a_0$, $R_2 = 2.953 a_0$ and $R_3 = 2.062 a_0$, differing 0.044 a_0 , 0.027 a_0 , and 0.008 a_0 from that of ref. 16, which is based on 1357 grid points with AVTZ basis set. While the internuclear distances of the R_1 , R_2 , and R_3 differ from the experimental results¹⁹ obtained by 0.007 a_0 , 0.0003 a_0 , and 0.023 a_0 , showing a high accuracy. It can be concluded from Table 2 that LM2–LM4 are all in long range, and both LM2 and LM3 correspond to the $\text{H}(^2S) + \text{CS}(X^1\Sigma^+)$ asymptote, while LM4 corresponds to the $\text{S}(^3P) + \text{CH}(X^2\Pi)$ asymptote. Figure 2(b) shows the contour plot of H–S–C linear stretching, in which the van der Waals local minimum (LM3), second-order saddle point (SP7), and transition state (TS7) can be observed. It is interesting to notice that the energy of the $\text{H}(^2S) + \text{CS}(X^1\Sigma^+)$ asymptote is lower than the $\text{C}(^3P) + \text{SH}(X^2\Pi)$ asymptote energy level, which indicates that the reaction $\text{H}(^2S) + \text{CS}(X^1\Sigma^+) \rightarrow \text{C}(^3P) + \text{SH}(X^2\Pi)$ is an endothermic one. The notable features in panel (c) are another van der Waals local minimum (LM4), two second-order saddle points (SP1 and SP2), and there are two transition states (TS6 and TS4). In the last panel, there is a deep well (TS5) about $-0.3486 E_h$, located at $R_1 = 4.928 a_0$, $R_2 = 2.916 a_0$ and $R_3 = 2.021 a_0$, which can be seen from Table 2. The TS5 and the $\text{CH}(X^2\Pi) + \text{S}(^3P)$ asymptote are connected by a second-order saddle point (SP3).

In order to illustrate the other stationary points on the new PES, a contour plot as a function of the C–H bond distance and the $\angle\text{HCS}$ is displayed in Fig. 3, in which the CS bond distance are optimized. The stationary points not appearing in Fig. 2 can be observed in Fig. 3, which are two deep minima (GM and LM1) corresponding to the stable HCS and HSC intermediates and the isomerization transition state (TS2) connecting these two minima is clearly seen from the new PES. The barrier height of TS2 is calculated to be 21.6 kcal mol^{-1} above the LM1, which is found to be well consistent with the results of Stoecklin *et al.*⁹. The GM well is found to be 37.8 kcal mol^{-1} below the LM1 well. The energy compares well with the result reported by Voronin¹⁶. It is interesting to notice the

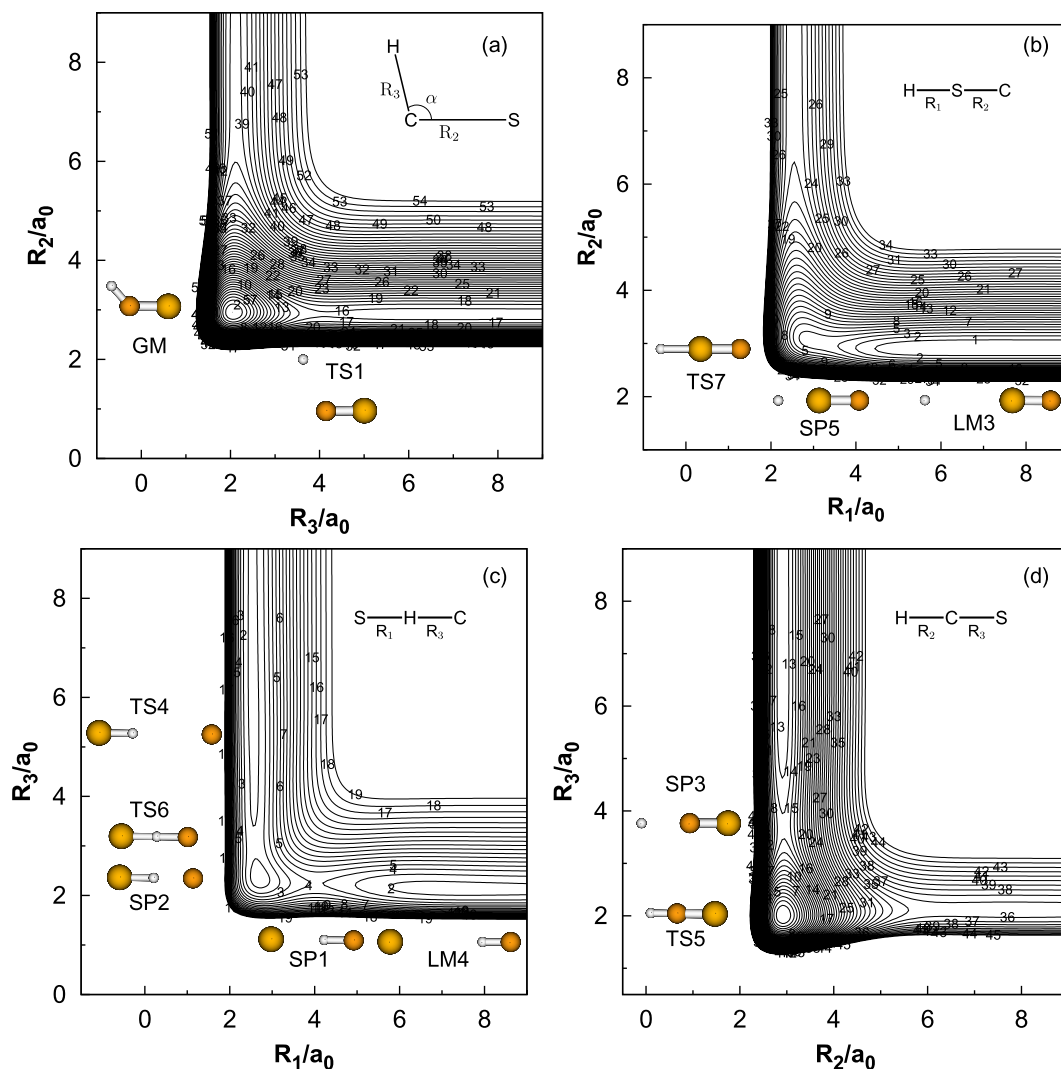


Figure 2. Contour plot for the ground-state PES of the HCS system. Contours are spaced by $0.006 E_h$, starting from $-0.3614 E_h$ in panel (a), $-0.2748 E_h$ in panel (b), $-0.1449 E_h$ in panel (c), and $-0.3424 E_h$ in panel (d).

existence of an entrance barrier for the H addition pathway to the CS molecule (or an exit barrier for the HCS/HSC \rightarrow H + CS dissociation). In another words, the TS1 connects the global minimum (GM) with the CS($X^1\Sigma^+$) + H(2S) asymptote, while TS3 connects the local minimum (LM1) with the CS($X^1\Sigma^+$) + H(2S) asymptote. A closer examination shows that the LM1 on the new PES is $16.75 \text{ kcal mol}^{-1}$ lower than the CS($X^1\Sigma^+$) + H(2S) asymptote, while Stoecklin *et al.*¹⁰ reported that the LM2 is $5.1 \text{ kcal mol}^{-1}$ above the CS($X^1\Sigma^+$) + H(2S) asymptote. The difference may be due to the different quality of PES. All major topographical features of the analytical potential energy surface function (APES) are probably better viewed in a relaxed triangular plot³⁴ utilizing scaled hyperspherical coordinates ($\beta^* = \beta/Q$ and $\gamma^* = \gamma/Q$), where the Q , β and γ are defined as

$$\begin{pmatrix} Q \\ \beta \\ \gamma \end{pmatrix} = \begin{pmatrix} 1 & 1 & 1 \\ 0 & \sqrt{3} & -\sqrt{3} \\ 2 & -1 & -1 \end{pmatrix} \begin{pmatrix} R_1^2 \\ R_2^2 \\ R_3^2 \end{pmatrix}. \quad (7)$$

As shown in Fig. 4, such a plot depicts in a physical way all the stationary points discussed above.

The minimum energy paths (MEPs) in different configurations (at a fixed $\angle\text{CSH}$ angle) are shown in Fig. 5. These MEPs represent the potential energy of HCS as a function of a suitable reaction coordinate defined as $R_{\text{SH}} - R_{\text{CS}}$, where R_{SH} and R_{CS} are the SH and CS internuclear distances, respectively. As shown in Fig. 5, R_{SH} approaches the SH equilibrium distance when the values of the reaction coordinate are in large negative values, whereas large positive values of the reaction coordinate correspond to R_{CS} approaching the CS equilibrium distance. It is shown that the reaction $\text{C}(^3P) + \text{SH}(X^2\Pi) \rightarrow \text{H}(^2S) + \text{CS}(X^1\Sigma^+)$ is highly exothermic, with the exothermicity being $\sim 84.3 \text{ kcal mol}^{-1}$, while Stoecklin *et al.*¹⁰ reported the exoergicity which took into account the

Feature	R_1/a_0	R_2/a_0	R_3/a_0	E/E_h	ω_1	ω_2	ω_3
HCS Minimum							
GM/CBS	4.596	2.953	2.062	-0.3614	3775.10	704.03	995.84
GM/AVQZ	4.598	2.966	2.058	-0.3589	3024	815	1214
GM/AVSZ	4.593	2.958	2.057	-0.3599	3024	810	1207
Theor. ¹⁶	4.64	2.98	2.07	—	3000.4	888.96	1143.52
Theor. ¹⁵	4.583	2.953	2.060	—	—	—	—
Exp. ¹⁹	4.589	2.953	2.039	—	—	—	—
LM1	2.545	3.078	4.486	-0.3011	2739.45	2961.07	481.82
LM2	7.481	2.911	6.029	-0.2750	3909.03	105.82	35.49
LM3	6.655	2.909	9.564	-0.2746	19.41	3932.13	18.49
LM4	7.029	9.170	2.142	-0.1359	21.28	207.20	907.16
HCS Transition state (TS)							
TS1	6.144	2.911	4.356	-0.2739	386.87	3881.57	150.44i
TS2	2.632	3.193	3.024	-0.2666	2863.37	1446.62	429.55i
TS3	3.868	2.921	5.418	-0.2686	612.68i	3703.78	267.56
TS4	2.554	8.561	6.007	-0.1408	83.26i	2599.65	38.73
TS5	4.929	2.917	2.011	-0.3486	629.74i	3884.24	1088.12
TS6	2.687	5.045	2.358	-0.1423	645.74i	1946.23	584.65
TS7	3.021	3.037	6.058	-0.2544	808.55i	2593.46	225.44
HCS Second-order saddle (SP)							
SP1	4.046	6.288	2.242	-0.1207	309.01i	845.76i	867.87
SP2	2.587	5.590	3.003	-0.1379	2473.22	485.10i	270.75i
SP3	6.609	2.927	3.682	-0.2633	409.72i	3751.14	353.53i
SP4	3.484	2.976	3.653	-0.2509	3358.95	1221.41i	4399.20i
SP5	3.128	3.028	6.146	-0.2544	731.97i	2597.81	215.75i

Table 2. Properties of stationary points on the fitted HCS(X^2A') PES (harmonic frequencies in cm^{-1}).

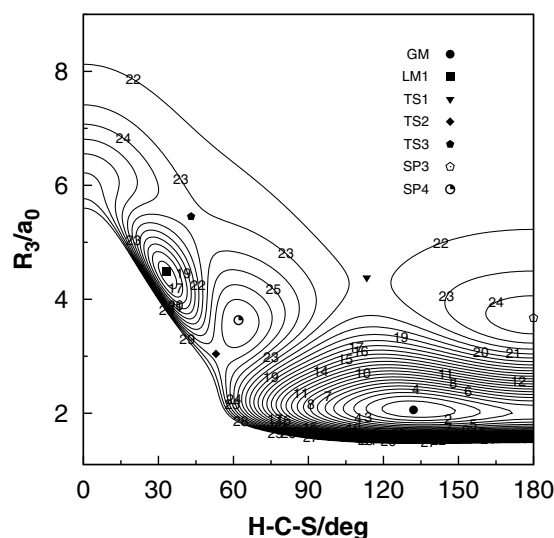


Figure 3. Contour map of the HCS PES plotted as a function of the C-H bond distance and the \angle HCS with an optimized CS bond length ($2.9078 a_0$). The contours are spaced by $0.004 E_h$, starting from $-0.3614 E_h$.

zero-point energy is $82.7 \text{ kcal mol}^{-1}$. It can be seen from this figure that the well is becoming shallow from \angle CSH angle 45° to 180° , and the deepest well is $\sim 16.2 \text{ kcal mol}^{-1}$ relative to the $\text{H}(^2S) + \text{CS}(X^1\Sigma^+)$ asymptote with the $R_{\text{SH}} = 3.483 a_0$ and $R_{\text{CS}} = 2.980 a_0$. Note further that the MEPs on the present PES has a shallow potential barrier in $\text{H}(^2S) + \text{CS}(X^1\Sigma^+)$ asymptote at \angle CSH angle 90° and 135° . This barrier can be assigned to be TS3 which connects the LM1 with the $\text{CS}(X^1\Sigma^+) + \text{H}(^2S)$ asymptote, with the barrier height being calculated to be $3.6 \text{ kcal mol}^{-1}$ higher than the $\text{CS}(X^1\Sigma^+) + \text{H}(^2S)$ asymptote. However, when the angle becomes smaller, the $\text{CS}(X^1\Sigma^+) + \text{H}(^2S)$ asymptote and GM are connected by the TS1, which is only $0.25 \text{ kcal mol}^{-1}$ higher than the $\text{CS}(X^1\Sigma^+) + \text{H}(^2S)$ asymptote.

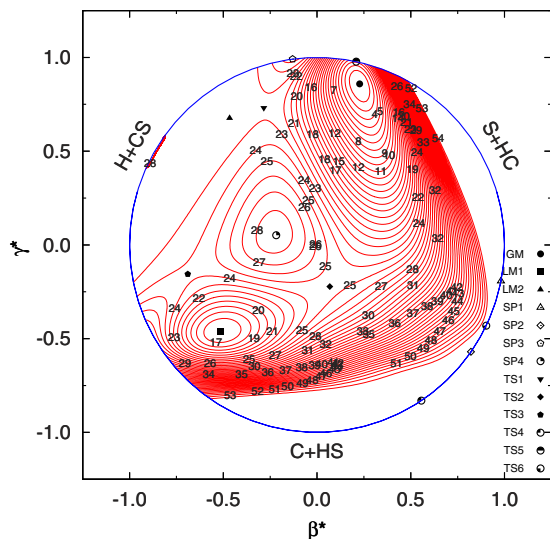


Figure 4. Relaxed triangular plot of new PES in hyperspherical coordinates. The location and symmetry of all stationary points are displayed. Contours equally spaced by $0.004E_h$, starting at $-0.3613E_h$.

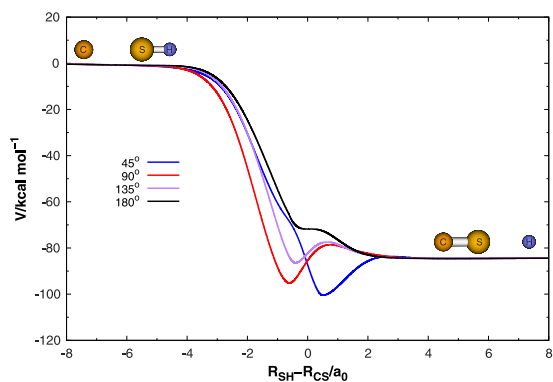


Figure 5. Minimum energy path for the $C(^3P) + SH(X^2II) \rightarrow H(^2S) + CS(X^1\Sigma^+)$ reaction calculated on new PES as a function of $R_{SH} - R_{CS}$ at the $\angle CSH$ angle 45° , 90° , 135° , and 180° .

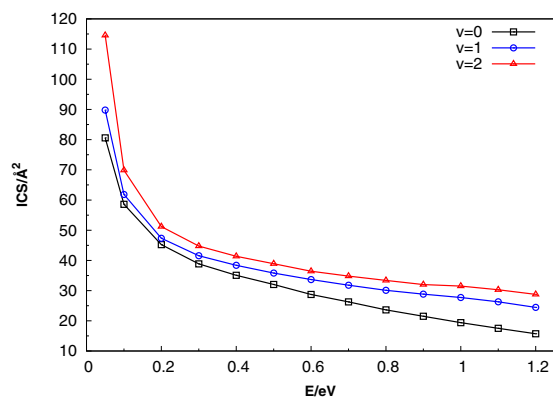


Figure 6. Calculated integral cross sections as a function of collision energy for the $C + SH(v=0, 1, 2; j=0)$.

Exploratory dynamic studies. Based on the present $HCS(X^2A')$ PES, we have calculated the integral cross-section (ICS), differential cross-section (DCS) and rate constants of $C + SH$. Figure 6 presents the QCT ICS as a function of different collision energies (0.05–1.2 eV) for $C(^3P) + SH(X^2II)$ ($v=0, 1, 2$;

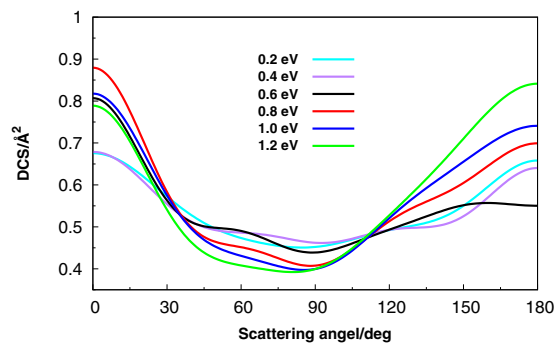


Figure 7. Differential cross section at different collision energies.

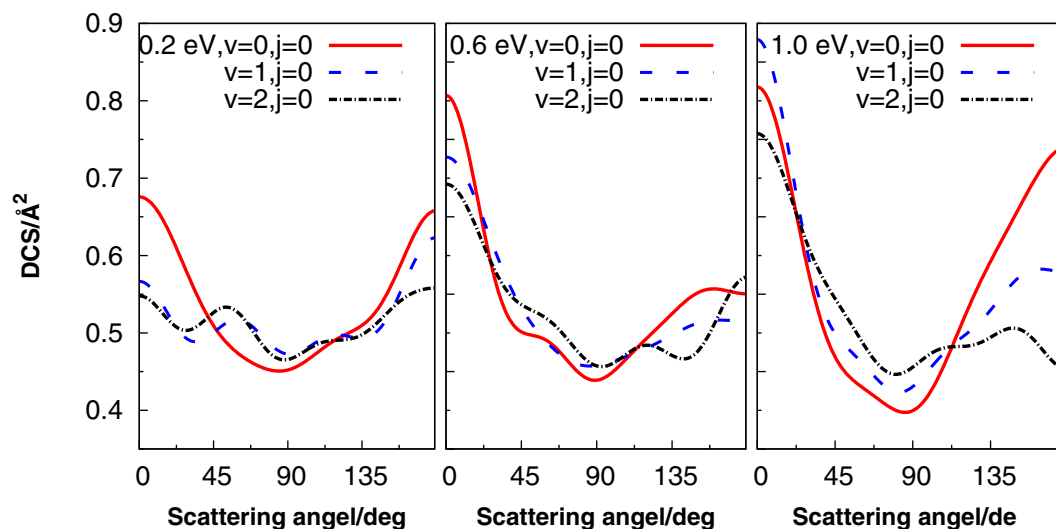


Figure 8. Differential cross section at different vibrational energy levels with fixed collision energies (0.2 eV, 0.6 eV, 1.0 eV).

$j=0$) \rightarrow $\text{H}^2\text{S} + \text{CS}(X^1\Sigma^+)$ reaction. An obvious decline can be seen in Fig. 6 as the collision energy increases, which is ascribed to the deep well and barrierless aspect of the present $\text{HCS}(X^2A')$ PES. As the collision energy increases, the ICS curve shows a rapidly decreasing trend from 0.05 eV to 0.2 eV, and relatively slow circumstance between 0.2 eV–1.2 eV when $\nu=0$. The trend of this curve is very similar to other exothermic reactions^{35–38}. In order to further investigate the effect of the reactant SH vibrational excitation on this reaction, we plotted the ICSs of $\text{C} + \text{SH}(\nu, j=0)$ reaction for $\nu=0, 1, 2$ in Fig. 6. We can see that the ICSs for the three vibrational states all decrease rapidly as the collision energy increases. As the vibrational quantum number increases, the ICSs for the $\nu=1, 2$ are all higher than that of the ground vibrational state, and the larger the vibrational quantum number, the higher the related ICSs. Thus, it can be concluded that SH vibration enhances the reactivity.

The so obtained ICSs are then used to calculate the rate constant of the title reaction at 300 K, which is $5.12 \times 10^{-13} \text{ cm}^3 \text{ molecule}^{-1} \text{ s}^{-1}$. Unfortunately, as far as we know, there is no experimental work reported on the rate constant. Thus, a direct comparison cannot be made between them. While, Voronin *et al.*¹⁶ and Stoelcllin's *et al.*¹¹ calculated the rate constant at the same temperature. The results of Voronin¹⁶ is $1.745 \times 10^{-13} \text{ cm}^3 \text{ molecule}^{-1} \text{ s}^{-1}$. The difference may be due to the different characteristics of the present PES and that of Voronin *et al.*¹⁶.

The DCSs offer an excellent opportunity to study the most familiar vector correlation between the reagent and product relative velocity ($k - k_0$). As shown in Fig. 7, it is clear that the DCS is dominated by scattering in both the forward and backward directions, which is consistent with the complex-forming mechanism for this reaction, and is similar to other exothermic reactions^{39,40}. None of the DCS is completely symmetrical, showing slightly backward bias at all six collision energies. The reason for the results may be that with the energy increasing, and the trap binding becoming small, when the centrifugal potential is approximately equal to the depth of the well, the trend of head to head collision dominant the reaction. So, backward scattering is slightly larger than the forward scattering. The DCSs of different vibrational energy levels with fixed collision energies (0.2 eV, 0.6 eV, 1.0 eV) are also plotted in Fig. 8. We can see that the vibrational excitation DCSs in both forward and backward are lower than that of the ground vibrational state. So we can conclude that the SH vibration inhibits the forward and backward scattering in the same collision energy.

Discussion

We have reported a globally accurate PES for the electronic ground state of HCS based on a wealth of *ab initio* energies calculated at MRCI(Q)/AVQZ and MRCI(Q)/AV5Z level of theory, which is expected to be realistic over the entire configuration space. Such raw energies are subsequently extrapolated to CBS limit. The properties of the major stationary points, including geometries, energies and vibrational frequencies have been characterized on the current HCS(X^2A') PES, showing good agreement with other theoretical and experimental results. The various topographical features of the current PES give an accurate description over the short and long range interactions. The present PES has been subsequently employed to carry out the QCT calculation of the ICS, DCS and the thermal rate constant for the reaction $C(^3P) + SH(X^2\Pi) \rightarrow H(^2S) + CS(X^1\Sigma^+)$. The present HCS(X^2A') PES is recommended for dynamic studies of $C(^3P) + SH(X^2\Pi)$ reaction in more detail,

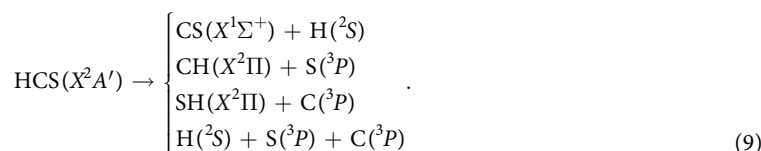
Methods

Analytical potential energy surface function. The APES for the HCS(X^2A') can be represented by MBE⁴¹, which is as follows:

$$V_{ABC} = \sum_A V_A^{(1)} + \sum_{AB} V_{AB}^{(2)}(R_{AB}) + V_{ABC}^{(3)}(R_{AB}, R_{AC}, R_{BC}), \quad (8)$$

in which the one-body term ($V_A^{(1)}$) is the energy of the separated atoms in their corresponding electronic state, usually ($\sum_A V_A^{(1)} = 0$) for all the atoms in their ground states, the two-body terms ($V_{AB}^{(2)}$) correspond to the diatomic PECs, including the nuclear repulsions, and the three-body term ($V_{ABC}^{(3)}$) takes into account the interactions between three atoms.

For the HCS(X^2A') PES, it follows the dissociation scheme as



Since $H(^2S)$, $C(^3P)$ and $S(^3P)$ are all in their ground states, the values of ($V_A^{(1)}$) can be set to zero, which is similar to other systems^{42–44}.

The terms ($V_{AB}^{(2)}$) involve the $\text{CS}(X^1\Sigma^+)$, $\text{CH}(X^2\Pi)$ and $\text{SH}(X^2\Pi)$, with their analytical expression being represented by the formalism developed by Aguado and Paniagua^{45,46}, and can be expressed as a sum of two terms corresponding to the short- and long-range potentials,

$$V_{AB}^{(2)} = V_{\text{short}}^{(2)} + V_{\text{long}}^{(2)}, \quad (10)$$

where

$$V_{\text{short}}^{(2)} = \frac{a_0}{R_{AB}} e^{-\beta_1^{(2)} R_{AB}}, \quad (11)$$

which warrants the diatomic potentials tending to infinite value when $R_{AB} \rightarrow 0$, and the long-range potentials which tend to zero as $R_{AB} \rightarrow \infty$ takes the following expression

$$V_{\text{long}}^{(2)} = \sum_{i=1}^n a_i \left(R_{AB} e^{-\beta_2^{(2)} R_{AB}} \right)^i. \quad (12)$$

The linear parameters a_i ($i = 1, 2, \dots, n$) and the nonlinear parameters β_i ($i = 1, 2$) in Eq. (11) and (12) are obtained by fitting the *ab initio* energies of the diatoms.

The three-body term ($V_{ABC}^{(3)}$) of the global potential in Eq. (8) can be written as M th-order polynomial^{45,46}

$$V_{ABC}^{(3)}(R_{AB}, R_{BC}, R_{AC}) = \sum_{j,k,l=0}^M C_{jkl} \rho_{AB}^j \rho_{AC}^k \rho_{BC}^l, \quad (13)$$

where $\rho_{AB} = R_{AB} e^{-\beta_{AB}^{(3)} R_{AB}}$, C_{jkl} and $\beta_{AB}^{(3)}$ are linear and nonlinear parameters, which are determined in the fitting procedure. The constraints $j+k+l \neq j \neq k \neq l$ and $j+k+l \leq M$ are employed to warrant that the three-body term becomes zero at all dissociation limits and when at least one of the internuclear distances is zero. M is set to be 9 in the present work, which results in a complete set of parameters to be determined amounts to a total number of 192 for linear coefficients C_{jkl} and 3 for nonlinear parameters (i.e., $\beta_{CH}^{(3)}$, $\beta_{SH}^{(3)}$ and $\beta_{CS}^{(3)}$). The root mean squared deviations (rmsd) values of the final PES with respect to all the fitted *ab initio* energies are gathered in Table 3. As shown in Table 3, a total of 5528 points have been used for the calibration procedure, thus covering a range up to 820 kcal/mol above the HCS global minimum. This table demonstrates that the final PES is able to fit the region of major chemical interest with a high accuracy (rmsd = 0.998 kcal/mol), including the global minimum and transition state for the C + SH dissociation process.

***Ab initio* electronic structure calculations.** The *ab initio* calculations have been carried out at the MRCI level^{47,48} of theory with the MOLPRO 2012 package⁴⁹, including the Davidson correction [MRCI(Q)]⁵⁰, using the

Energy	N^a	rmsd	$N >_{\text{rmsd}}^b$
10	15	0.310	5
20	36	0.284	12
30	70	0.298	21
40	110	0.392	29
50	187	0.719	37
60	765	0.615	148
70	936	0.761	207
80	1085	0.794	251
90	1412	0.832	337
100	1897	0.819	544
200	4540	0.937	1119
400	4963	0.955	1249
600	5423	0.974	1362
820	5528	0.988	1393

Table 3. Root-mean-square deviations (in kcal mol⁻¹) of the PES. ^aNumber of points in the indicated energy range. ^bNumber of points with an energy deviation large than the rmsd.

full valence CASSCF⁵¹ wave function as the reference. The AVQZ and AV5Z atomic basis sets of Dunning^{52,53} have been employed. A grid of 5528 *ab initio* points have been chosen to map the PES over the H – CS region defined by $2.0 \leq R_{\text{CS}}/a_0 \leq 4.5$, $0.6 \leq r_{\text{H-CS}}/a_0 \leq 15$, and $0.0 \leq \gamma/\text{deg} \leq 180$, C – SH region by $2.0 \leq R_{\text{SH}}/a_0 \leq 4.0$, $0.6 \leq r_{\text{C-SH}}/a_0 \leq 15$, and $0.0 \leq \gamma/\text{deg} \leq 180$, and S – CH region by $1.5 \leq R_{\text{CH}}/a_0 \leq 4.0$, $0.6 \leq r_{\text{S-CH}}/a_0 \leq 15$, and $0.0 \leq \gamma/\text{deg} \leq 180$. R , r and γ are the atom-diatom Jacobi coordinates. C_s point group symmetry is employed in the *ab initio* calculation, which holds two irreducible representations, namely, A' and A'' . For HCS(X^2A''), seven A' and two A'' symmetry molecular orbitals (MOs) are determined as the active space, amounting to a total of 338 ($207A' + 131A''$) configuration state functions.

Extrapolation to CBS Limit. Subsequently, the *ab initio* energies calculated in this way were extrapolated to the CBS limit. The MRCI(Q) energy is treated as usual in split form by writing⁵⁴

$$E_X(\mathbf{R}) = E_X^{\text{CAS}}(\mathbf{R}) + E_X^{\text{dc}}(\mathbf{R}), \quad (14)$$

where the subscript X indicates that the *ab initio* energies are calculated in the AVXZ basis, and the superscript dc and CAS denote the dynamical correlation energy and complete-active space energy, respectively. Note that all extrapolations are carried pointwise, and hence the vector \mathbf{R} of the nuclear geometrical coordinates will be omitted for simplicity. $X = (Q, 5)$ is employed in the present work, which is denoted as USTE(Q, 5).

The CAS energies are extrapolated to the CBS limit by utilizing the two-point extrapolation scheme proposed by Karton and Martin⁵⁵ and validated by Varandas⁵⁴ in the extrapolation of the CASSCF energies

$$E_X^{\text{CAS}} = E_\infty^{\text{CAS}} + B/X^\alpha, \quad (15)$$

where α is a predefined constant. Being a two-parameter protocol (E_∞^{CAS} , B), a minimum of two raw energies will be required for the extrapolation. Specifically, Eq. (15) will be calibrated from the CAS/AV(Q, 5)Z energy pairs, using a value of $\alpha = 5.34$, which has been found to be an optimal value when extrapolating HF energies to the CBS limit.

The USTE method^{54,56} has been successfully applied to extrapolate the dc energies, with its formalism been written as

$$E_X^{\text{dc}} = E_\infty^{\text{dc}} + \frac{A_3}{(X + \alpha)^3} + \frac{A_5}{(X + \alpha)^5}, \quad (16)$$

and here,

$$A_5 = A_5(0) + cA_3^{(5/4)}, \quad (17)$$

with $A_5(0) = 0.0037685459$, $c = -1.17847713$ and $\alpha = -3/8$ as the universal-type parameters^{54,56}. Thus, Eq. (16) can be reduced into a (E_∞^{dc} , A_3) two-parameter rule, which is actually used for the practical procedure of the extrapolation.

Reaction Dynamics. By employing the present HCS(X^2A') PES, the reaction of $\text{C}(^3P) + \text{SH}(X^2\Pi) \rightarrow \text{H}(^2S) + \text{CS}(X^1\Sigma^+)$ is investigated by QCT⁵⁷⁻⁶¹ calculations.

In present work, the collision energy is chosen to be 0.05–1.2 eV and batches of 100000 trajectories are run for each collision energy. The trajectories are initiated at a distance of 20 Å between the C atom and the SH diatom, and the integration step size is 0.1 fs. The maximal impact parameters b_{max} are optimized before running the trajectories. The ICS is then calculated as

$$\sigma = \pi b_{\max}^2 \frac{N_r}{N}, \quad (18)$$

where N_r is the number of reactive trajectories in a total number of N , and b_{\max} is the maximal value of the impact parameters.

The rate constant $k(T)$ calculated with the ICS and Boltzmann integration over the collision energy is given by

$$k(T) = f(T) \sqrt{\frac{8k_B T}{\pi \mu_R}} (k_B T)^{-2} \int_0^\infty E \sigma(E) \exp\left(-\frac{E}{k_B T}\right) dE, \quad (19)$$

where k_B is the Boltzmann constant, E is the collision energy, and $f(T)$ is the electronic degeneracies of reagents and products which can be expressed as ref. 16

$$f(T) = \frac{2}{(1 + 3 \exp(-23.6/T) + 5 \exp(-62.59/T)) \cdot (2 + 2 \exp(-542.43/T))}. \quad (20)$$

The distribution function $P(\theta_r)$, which describes the k - k' correlation, is expanded in a series of Legendre polynomials^{57,62,63}

$$P(\theta_r) = \frac{1}{2} \sum_k (2k + 1) a_0^{(k)} P_k(\cos \theta_r), \quad (21)$$

where

$$a_0^{(k)} = \int_0^\pi p(\theta_r) P_k(\cos \theta_r) \sin \theta_r d\theta_r = \langle P_k(\cos \theta_r) \rangle. \quad (22)$$

The coefficients $a_0^{(k)}$ are called orientation parameter (k is odd) or alignment parameter (k is even).

References

- Kaiser, R. I., Sun, W. & Suits, A. G. Crossed beam reaction of atomic carbon $C(^3P_j)$ with hydrogen sulfide, $H_2S(X^1A_1)$: Observation of the thioformyl radical, $HCS(X^2A')$. *J. Chem. Phys.* **106**, 5288–5291 (1997).
- Lee, H. H., Bettens, R. P. A. & Herbst, E. Fractional abundances of molecules in dense interstellar clouds: A compendium of recent model results. *Astron. Astrophys. Suppl. Ser.* **119**, 111–114 (1996).
- Ruscic, B. & Berkowitz, J. Photoionization mass spectrometry of CH_2S and HCS . *J. Chem. Phys.* **98**, 2568–2579 (1993).
- Kaiser, R. I., Ochsenfeld, C., Head-Gordon, M. & Lee, Y. T. The Formation of HCS and $HCSH$ molecules and their role in the collision of comet Shoemaker-Levy 9 with Jupiter. *Science* **279**, 1181–1184 (1998).
- Kaiser, R. I., Ochsenfeld, C., Head-Gordon, M. & Lee, Y. T. Crossed-beam reaction of carbon atoms with sulfur containing molecules. I. Chemical dynamics of thioformyl $HCS(X^2A')$ formation from reaction of $C(^3P_j)$ with hydrogen sulfide, $H_2S(X^1A_1)$. *J. Chem. Phys.* **110**, 2391–2403 (1999).
- Puzzarini, C. The HCS/HSC and HCS^+/HSC^+ systems: molecular properties, isomerization, and energetics. *J. Chem. Phys.* **123**, 024313–14 (2005).
- Goddard, J. D. The structure of the thioformyl radical, HCS . *Chem. Phys. Lett.* **102**, 224–226 (1983).
- Pope, S. A., Hillier, I. H. & Guest, M. F. Rearrangement and fragmentation processes on the potential energy surfaces of thioformaldehyde molecule and cation. *J. Amer. Chem. Soc.* **107**, 3789–3800 (1985).
- Stoecklin, T., Halvick, P. & Rayez, J. Theoretical study of the reaction $C(^3P) + SH(X^2II)$. Part I. Semi-quantitative determination of some parts of the potential energy surfaces. *J. Mol. Structure: THEOCHEM* **163**, 267–283 (1988).
- Stoecklin, T., Rayez, J. & Duguay, B. Theoretical study of the reaction $C(^3P) + SH(X^2II)$. III. Two analytic models of the lowest potential energy surface. *Chem. Phys.* **148**, 381–397 (1990).
- Stoecklin, T., Rayez, J. & Duguay, B. Theoretical study of the reaction $C(^3P) + SH(X^2II)$. IV. A quasi-classical trajectory study of the reaction at 300 K. *Chem. Phys.* **148**, 399–409 (1990).
- Senekowitsch, J., Carter, S., Rosmus, P. & Werner, H. J. Potential energy and dipole moment functions of the HCS radical. *Chem. Phys.* **147**, 281–292 (1990).
- Curtiss, L. A., Nobes, R. H., Pople, J. A. & Radom, L. Theoretical study of the organosulfur systems CSH_n ($n = 0-4$) and CSH_n^+ ($n = 0-5$): Dissociation energies, ionization energies, and enthalpies of formation. *J. Chem. Phys.* **97**, 6766–6773 (1992).
- Ochsenfeld, C., Kaiser, R. I., Lee, Y. T. & Head-Gordon, M. Coupled-cluster *ab initio* investigation of singlet/triplet CH_2S isomers and the reaction of atomic carbon with hydrogen sulfide to HCS/HSC . *J. Chem. Phys.* **110**, 9982–9988 (1999).
- Chen, B. Z. & Huang, M. B. Hyperfine structure in HCS and related radicals: a theoretical study. *Chem. Phys. Lett.* **308**, 256–262 (1999).
- Voronin, A. Analytical global potential energy surface for the X^2A' state of HCS . *Chem. Phys.* **297**, 49–54 (2004).
- Mitrushchenkov, A., Linguerrri, R., Rosmus, P. & Maier, J. Alteration of the spin-orbit coupling in the 2II ground state of HC_nS ($n = 1-12$) radicals. *Mol. Phys.* **107**, 1549–1553 (2009).
- Habara, H. *et al.* Fourier transform millimeter-wave spectroscopy of the HCS radical in the $^2A'$ ground electronic state. *J. Chem. Phys.* **108**, 8859–8863 (1998).
- Habara, H., Yamamoto, S. & Amano, T. Submillimeter-wave spectra of HCS and DCS . *J. Chem. Phys.* **116**, 9232–9238 (2002).
- Habara, H. & Yamamoto, S. Microwave spectrum and molecular structure of the HSC radical. *J. Chem. Phys.* **112**, 10905–10911 (2000).
- Habara, H. & Yamamoto, S. The ^{13}C hyperfine constants of HCS and HSC studied by microwave spectroscopy. *J. Mol. Spectrosc.* **219**, 30–36 (2003).
- Song, Y. Z. & Varandas, A. J. C. Accurate double many-body expansion potential energy surface for ground-state HS_2 based on *ab initio* data extrapolated to the complete basis set limit. *J. Phys. Chem. A* **115**, 5274–5283 (2011).
- Li, Y. Q., Ma, F. C. & Sun, M. T. Accurate *ab initio*-based adiabatic global potential energy surface for the $2^2A''$ state of NH_2 by extrapolation to the complete basis set limit. *J. Chem. Phys.* **139**, 154305-1–7 (2013).
- Li, Y. Q. *et al.* Accurate Double Many-Body Expansion Potential Energy Surface by Extrapolation to the Complete Basis Set Limit and Dynamics Calculations for Ground State of NH_2 . *J. Comput. Chem.* **34**, 1686–1696 (2013).

25. Song, Y. Z. & Varandas, A. J. C. Accurate *ab initio* double many-body expansion potential energy surface for ground-state H₂S by extrapolated to the complete basis set limit. *J. Chem. Phys.* **130**, 134317-1–10 (2009).
26. Zhang, L. L., Gao, S. B., Meng, Q. T. & Song, Y. Z. Accurate *ab initio*-based analytical potential energy function for S₂($\bar{a}^1\Delta_g$) via extrapolation to the complete basis set limit. *Chin. Phys. B.* **24**, 013101-1–7 (2015).
27. Zhang, L. L., Zhang, J., Meng, Q. T. & Song, Y. Z. Accurate potential energy curve and spectroscopic properties of S₂($b^1\Sigma_g^+$) via extrapolation to the complete basis set limit. *Phys. Scri.* **90**, 035403 (2015).
28. Peterson, K. A., Mitrushchenkov, A. & Francisco, J. S. A. Theoretical study of the spectroscopic properties of the ground and first excited electronic state of HS₂. *Chem. Phys.* **346**, 34–44 (2008).
29. Shi, D. H. *et al.* Accurate analytic potential energy function and spectroscopic study for CH(X²Π) radical using coupled-cluster theory in combination with the correlation-consistent quintuple basis set. *J. Mol. Struct.: THEOCHEM* **860**, 101–105 (2008).
30. Kalemios, A., Mavridis, A. & Metropoulos, A. An accurate description of the ground and excited states of CH. *J. Chem. Phys.* **111**, 9536–9548 (1999).
31. Hirata, S. *et al.* Third-order Douglas-Kroll relativistic coupled-cluster theory through connected single, double, triple, and quadruple substitutions: Applications to diatomic and triatomic hydrides. *J. Chem. Phys.* **120**, 3297–3310 (2004).
32. Shi, D. H. *et al.* MRCI study on potential energy curves, spectroscopic parameters and rovibrational energy levels of CS(X¹Σ⁺). *J. Mol. Struct.: THEOCHEM* **945**, 1–7 (2010).
33. Molecular spectra and molecular structure constants of diatomic molecules (van nostrand reinhold, new york, 1979). Huber, K. P.; Herzberg, G.
34. Varandas, A. J. C. A useful triangular plot of triatomic potential energy surfaces. *Chem. Phys. Lett.* **138**, 455–461 (1987).
35. Lin, S. Y. & Guo, H. Quantum statistical and wave packet studies of insertion reactions of S(¹D) with H₂, HD, and D₂. *J. Chem. Phys.* **122**, 074304–9 (2005).
36. Sun, Z. P. *et al.* Quantum reaction dynamics of the C(¹D) + H₂(D₂) → CH(D) + H(D) on a new potential energy surface. *J. Chem. Phys.* **139**, 014306–6 (2013).
37. Gao, S. B., Zhang, J., Song, Y. Z. & Meng, Q. T. Cross sections for vibrational inhibition at low collision energies for the reaction H + Li₂(X¹Σ⁺) → Li + LiH(X¹Σ⁺). *Eur. Phys. J. D.* **69**, 1–6 (2015).
38. Gao, S. B., Zhang, L. L., Song, Y. Z. & Meng, Q. T. Coriolis coupling effects in the H + Li₂(X¹Σ⁺) → LiH(X¹Σ⁺) + Li reaction: A time-dependent wave packet investigation. *Chem. Phys. Lett.* **651**, 233–237 (2016).
39. Zhao, J. Quasi-classical trajectory study of the O(¹D) + HF reaction dynamics on 1¹A' potential energy surface. *Can. J. Chem.* **89**, 650–656 (2011).
40. Zhang, Y. Y. *et al.* Theoretical prediction of energy dependence for D + BrO → DBr + O reaction: The rate constant and product rotational polarization. *Chin. Phys. B.* **24**, 038201-1–6 (2015).
41. Varandas, A. J. C. Intermolecular and intramolecular potentials: topographical aspects, calculation, and functional representation via a DMBE expansion method. *Adv. Chem. Phys.* **74**, 255–337 (1988).
42. Song, Y. Z. *et al.* Globally accurate *ab initio* based potential energy surface of H₂O⁺ (X⁴A''). *Chin. Phys. B.* **24**, 063101-1–8 (2015).
43. Li, Y. Q., Zhang, P. Y. & Han, K. L. Accurate high level *ab initio*-based global potential energy surface and dynamics calculations for ground state of CH₃⁺. *J. Chem. Phys.* **142**, 124302-1–6 (2015).
44. Li, Y. Q. *et al.* *Ab initio*-based double many-body expansion potential energy surface for the first excited triplet state of the ammonia molecule. *J. Chem. Phys.* **136**, 194705-1–8 (2012).
45. Aguado, A. & Paniagua, M. A new functional form to obtain analytical potentials of triatomic molecules. *J. Chem. Phys.* **96**, 1265–1275 (1992).
46. Aguado, A., Tablero, C. & Paniagua, M. Global fit of *ab initio* potential energy surfaces I. Triatomic systems. *Comp. Phys. Comm.* **108**, 259–266 (1998).
47. Werner, H. J. & Knowles, P. J. An efficient internally contracted multiconfiguration reference CI method. *J. Chem. Phys.* **89**, 5803–5814 (1988).
48. Knowles, P. J. & Werner, H.-J. An efficient method for the evaluation of coupling coefficients in configuration interaction calculations. *Chem. Phys. Lett.* **145**, 514–522 (1988).
49. Werner, H. J. *et al.* Molpro: a general-purpose quantum chemistry program package. *Wires. Comput. Mol. Sci.* **2**, 242–253 (2012).
50. Langhoff, S. R. & Davidson, E. R. Configuration interaction calculations on the nitrogen molecule. *Int. J. Quantum Chem.* **8**, 61–72 (1974).
51. Knowles, P. J. & Werner, H. J. An efficient second order MCSCF method for long configuration expansions. *Chem. Phys. Lett.* **115**, 259–267 (1985).
52. Dunning, T. H. Jr. Gaussian basis sets for use in correlated molecular calculations. I. The atoms boron through neon and hydrogen. *J. Chem. Phys.* **90**, 1007–1023 (1989).
53. Kendall, R. A., Dunning, T. H. Jr. & Harrison, R. J. Electron affinities of the first-row atoms revisited. Systematic basis sets and wave functions. *J. Chem. Phys.* **96**, 6769–6806 (1992).
54. Varandas, A. J. C. Extrapolating to one-electron basis-set limit in electronic structure calculations. *J. Chem. Phys.* **126**, 244105–244119 (2007).
55. Karton, A. & Martin, J. M. L. Comment on “Estimating the Hartree-Fock limit from finite basis set calculations”. *Theor. Chem. ACC.* **115**, 330–333 (2006).
56. Varandas, A. J. C. Basis-set extrapolation of the correlation energy. *J. Chem. Phys.* **113**, 8880–8887 (2000).
57. Han, K. L., He, G. Z. & Lou, N. Q. Effect of location of energy barrier on the product alignment of reaction A + BC. *J. Chem. Phys.* **105**, 8699–8704 (1996).
58. Aoiz, F. J., Brouard, M. & Enriquez, P. A. Product rotational polarization in photon-initiated bimolecular reactions. *J. Chem. Phys.* **105**, 4964–4982 (1996).
59. Aoiz, F. J., Banares, L. & Herrero, V. J. Recent results from quasiclassical trajectory computations of elementary chemical reactions. *J. Chem. Soc., Faraday Trans.* **94**, 2483–2500 (1998).
60. Aoiz, F. J., Sáez-Rábanos, V., Martínez-Haya, B. & González-Lezana, T. Quasiclassical determination of reaction probabilities as a function of the total angular momentum. *J. Chem. Phys.* **123**, 094101-14 (2005).
61. Hu, W. & Schatz, G. C. Theories of reactive scattering. *J. Chem. Phys.* **125**, 132301–15 (2006).
62. Wang, M. L., Han, K. L. & He, G. Z. Product rotational polarization in the photoinitiated bimolecular reaction A + BC → AB + C on attractive, mixed and repulsive surfaces. *J. Chem. Phys.* **109**, 5446–5454 (1998).
63. Wang, M. L., Han, K. L. & He, G. Z. Product Rotational Polarization in Photo-initiated Bimolecular Reactions A + BC: Dependence on the Character of the Potential Energy Surface for Different Mass Combinations. *J. Phys. Chem. A.* **102**, 10204–10210 (1998).

Acknowledgements

This work was supported by National Natural Science Foundation of China (Grant No 11674198), National Natural Science Foundation of China (Grant No 11304185), Taishan scholar project of Shandong Province, Shandong Provincial Natural Science Foundation (Grant No ZR2014AM022), Shandong Province Higher

Educational Science and Technology Program (Grant No J15LJ03), China Postdoctoral Science Foundation (Grant No 2014M561957), and Post-doctoral Innovation Project of Shandong Province (Grant No 201402013).

Author Contributions

Q.T.M. supervised the project, L.L.Z. calculated the *ab initio* energy points, Y.Z.S. and L.L.Z. fitted the potential energy surface, S.B.G. performed the QCT calculations, Y.Z.S. and L.L.Z. wrote the paper.

Additional Information

Competing financial interests: The authors declare no competing financial interests.

How to cite this article: Song, Y.-Z. *et al.* Globally accurate potential energy surface for the ground-state HCS (X^2A') and its use in reaction dynamics. *Sci. Rep.* **6**, 37734; doi: 10.1038/srep37734 (2016).

Publisher's note: Springer Nature remains neutral with regard to jurisdictional claims in published maps and institutional affiliations.



This work is licensed under a Creative Commons Attribution 4.0 International License. The images or other third party material in this article are included in the article's Creative Commons license, unless indicated otherwise in the credit line; if the material is not included under the Creative Commons license, users will need to obtain permission from the license holder to reproduce the material. To view a copy of this license, visit <http://creativecommons.org/licenses/by/4.0/>

© The Author(s) 2016